Unclassified
SECURITY CLASSIFICATION OF THIS PAGE

REPORT DOCUMENTATION PAGE

Form Approved
OMB No. 0704-0188

1a. REPORT SECURITY CLASSIFICATION: UNCLASSIFIED	1b. RESTRICTIVE MARKINGS
2a. SECURITY CLASSIFICATION AUTHORITY	3. DISTRIBUTION/AVAILABILITY OF REPORT: Approved for public release, distribution unlimited
2b. DECLASSIFICATION/DOWNGRADING SCHEDULE	
4. PERFORMING ORGANIZATION REPORT NUMBER(S): FMRL-TR94-1	5. MONITORING ORGANIZATION REPORT NUMBER(S): AFOSR-TR- 94 0162
6a. NAME OF PERFORMING ORGANIZATION: Florida State University, Dept. of Mechanical Engineering (6b. OFFICE SYMBOL (If applicable))	7a. NAME OF MONITORING ORGANIZATION: Air Force Office of Scientific Research, Division of Aerospace Sciences
6c. ADDRESS (City, State, and ZIP Code): PO Box 2175, Tallahassee, FL 32316	7b. ADDRESS (City, State, and ZIP Code): Bolling AFB, Washington, DC 20332-6448
8a. NAME OF FUNDING/SPONSORING ORGANIZATION: AFOSR (8b. OFFICE SYMBOL (If applicable): NA)	9. PROCUREMENT INSTRUMENT IDENTIFICATION NUMBER: F49620-92-J-0426
8c. ADDRESS (City, State, and ZIP Code): AFOSR/NA, Bolling AFB DC 20332-6448	10. SOURCE OF FUNDING NUMBERS: PROGRAM ELEMENT NO. 61102F; PROJECT NO. 2307; TASK NO. B5; WORK UNIT ACCESSION NO.

11. TITLE (Include Security Classification)
An Experimental Investigation of Active Control of Thrust Vectoring Nozzle Flow Fields

12. PERSONAL AUTHOR(S)
Strykowski, PJ and Krothapalli, A

13a. TYPE OF REPORT	13b. TIME COVERED	14. DATE OF REPORT (Year, Month, Day)	15. PAGE COUNT
FINAL	FROM 92/07/15 TO 93/07/15	01/27/94	30

16. SUPPLEMENTARY NOTATION

17. COSATI CODES			18. SUBJECT TERMS (Continue on reverse if necessary and identify by block number)
FIELD	GROUP	SUB-GROUP	THRUST VECTORING NOZZLE; ACTIVE CONTROL

19. ABSTRACT (Continue on reverse if necessary and identify by block number)
Fluidic thrust vector control is examined in a supersonic rectangular jet having a 4:1 aspect ratio. Experiments conducted at a Mach number of 2 reveal that the thrust vector angle of the jet can be continuously varied by up to at least 16° by applying a counterflowing stream to one of the primary jet shear layers. A technique using counterflow eliminates the bistable response known to plague fluidic elements and is shown to be effective in both hot and cold supersonic jets. Results are presented for jet stagnation temperatures between 300°K and 670°K. Measurements indicate that the thrust vector control is both efficient as well as a linear function of the static pressure developed in the counterflowing stream. The typical power required to vector the jet at 16 degrees was estimated to be less than 1% of the power developed in the primary jet. Thrust vector control employing counterflow has several advantages over current technologies, the most important of which is the elimination of movable control surfaces which add considerable weight to the aircraft.

20. DISTRIBUTION/AVAILABILITY OF ABSTRACT	21. ABSTRACT SECURITY CLASSIFICATION
☐ UNCLASSIFIED/UNLIMITED ☒ SAME AS RPT. ☐ DTIC USERS	
22a. NAME OF RESPONSIBLE INDIVIDUAL: DR J.M. McMichael	22b. TELEPHONE (Include Area Code): 202-767-4936 — 22c. OFFICE SYMBOL: NA

DD Form 1473, JUN 86 — Previous editions are obsolete. — SECURITY CLASSIFICATION OF THIS PAGE

UNCLASSIFIED

An Experimental Investigation of Active Control of Thrust Vectoring Nozzle Flow Fields

by

P.J. STRYKOWSKI* and A. KROTHAPALLI†

*Department of Mechanical Engineering
The University of Minnesota,
Minneapolis, Minnesota 55455

†Department of Mechanical Engineering
FAMU/FSU College of Engineering
Florida A&M University and Florida State University,
Tallahassee, Florida 32316

Contract # F49620-92-J-0426

Prepared for

Air Force Office of Scientific Research
Bolling Air Force Base, Washington DC 20332
Final Report for the Period July 15, 1992 - July 15, 1993

An Experimental Investigation of Active Control of Thrust Vectoring Nozzle Flow Fields

P.J. STRYKOWSKI* and A. KROTHAPALLI†

*University of Minnesota, Minneapolis, Minnesota 55455

†Florida A&M University and Florida State University, Tallahassee, Florida 32316

Abstract

Fluidic thrust vector control is examined in a supersonic rectangular jet having a 4:1 aspect ratio. Experiments conducted at a Mach number of two reveal that the thrust vector angle of the jet can be continuously varied up to at least 16 degrees by applying a counterflowing stream to one of the primary jet shear layers. A technique using counterflow eliminates the bistable response known to plague fluidic elements and is shown to be effective in both hot and cold supersonic jets. Results are presented for jet stagnation temperatures between 300 and 670 Kelvin. Measurements indicate that the thrust vector control is both efficient as well as a linear function of the static pressure developed in the counterflowing stream. The typical power required to vector the jet at 16 degrees was estimated to be less than 1% of the power developed in the primary jet. Thrust vector control employing counterflow has several advantages over current technologies the most important of which is the elimination of movable control surfaces which add considerable weight to the aircraft.

* Associate Professor, Department of Mechanical Engineering

† Don Fuqua Professor and Chairman, Department of Mechanical Engineering.

Introduction

It is expected that the performance of the next generation of advanced fighter aircraft will depend on the successful development of multi-axis thrust vectoring nozzles. Thrust vector control has several advantages over maneuverability strategies based on movable aircraft surfaces on the wings and tail structure, in particular post-stall performance, reduced take-off distances and weight, and overall combat agility. However, many of the promising strategies currently under investigation require complicated hardware to redirect the engine exhaust. This hardware typically consists of movable "feathers" which will add considerable weight to the aircraft and undoubtedly be expensive in terms of drag penalty and time response. In this paper we will describe the operation of a fluidic thrust vectoring nozzle which relies on counterflow to redirect the jet exhaust. Fluidic thrust vector control has the advantage over existing technologies in that the control surfaces are stationary and are not directly exposed to the high temperature gases. The present approach also eliminates bistable operation which is known to limit the utility of many fluidic nozzle designs.

Technology demonstrator aircraft employing first generation vectoring nozzles have already proven the advantages of thrust vectoring under flight conditions. These early vectoring nozzles have developed along two different lines; the two-dimensional, convergent-divergent (2-D/C-D) nozzles with pitch vectoring and the axisymmetric nozzles with multi-axis vectoring. Vectoring nozzles of the 2-D/C-D type were first flown on the USAF STOL and Maneuvering Technologies Demonstrator (S/MTD) program. The twin Pratt and Whitney (P&W) nozzles demonstrated significant increased pitch rate and decreased takeoff roll of the modified F-15 aircraft using thrust vectoring. Application of vectoring 2-D/C-D nozzles continues through P&W's incorporation of them on the F-22. Multi-axis vectoring is currently being explored on the NASA F/A-18 High Alpha Research Vehicle (HARV) and the X-31 aircraft. The multi-axis vectoring capability has given both of these demonstrators increased roll rates and enhanced maneuverability at low speed, high angle of attack flight conditions. Both the F/A-18/HARV and the X-31 aircraft achieve multi-axis vectoring by a simple system of three vanes arrayed around each nozzle exit.

While these flight demonstration nozzles proved the effectiveness of vectoring, aircraft integration issues such as weight and external drag, particularly in the case of vane systems, were of secondary concern. In order to address these issues, industry is exploring several new vectoring nozzle concepts. General Electric (GE) continues to develop the 2-D/C-D vectoring nozzle concepts in light of the F-22 program. Sub-scale testing is currently assessing weight and ejector cooling schemes[1] in order to reduce the associated penalties with these nozzles.

Lately, much emphasis has been placed in further developing multi-axis vectoring nozzle concepts so that their advantages can be fully employed on future aircraft. Most notable of these efforts are GE's Axisymmetric Vectoring Exhaust Nozzle[2] (AVEN) and P&W's Pitch/Yaw Balanced Beam Nozzle (P/Y BBN). These concepts retain the light weight design of current axisymmetric nozzles but allow deflection of the divergent section flaps in any direction through added actuation and control hardware. Also of note is P&W's Spherical Convergent Flap Nozzle (SFCN). This nozzle has a rectangular exit but the hinge station is circular in shape. The configuration accommodates a spherical convergent section which allows vectoring in both pitch and yaw axes and also a 40% reduction in weight over the rectangular nozzles employed by the S/MTD. Scale testing by McDonnell Aircraft Company (MCAIR) and P&W has shown that the P/Y BBN and SFCN vectoring nozzle concepts have external drag levels comparable to current non-vectoring nozzles.[3] These multi-axis vectoring concepts have yet to be incorporated into full scale aircraft for flight testing, leaving the complete integration issue in question.

While vectoring jets by using variable nozzle geometry is rapidly maturing, using fluidic control of the jet to achieve vectoring has been pursued over the years with varying success. Most of the early work on fluidic jet control was carried out in the development of fluid-jet amplifiers. Studies by Olsen,[4] Comparin et al.[5] and Warren[6] showed that small jets could be easily directed through the use of secondary air injection and side walls at the jet exit. Since the primary purpose of these studies was to show the feasibility of such configurations for logic control devices, these fluidic control schemes were bistable in nature, thus making them unusable for aircraft control

applications. However, these early studies proved that jets could be effectively controlled without moving surfaces.

Fluidic control vectoring methods have also been tested on a larger scale for the application of missile or aircraft control. One such scheme is called Boundary-Layer Thrust Vector Control[7,8] (BLTVC). The BLTVC concept consists of an overexpanded nozzle with control ports placed around the perimeter of the divergent section. In order to vector the jet, one of the ports is vented to ambient air, the jet separates from this side of the nozzle resulting in vectored thrust. This technique depends on the ambient pressure being greater than the pressure in the diverging region of the nozzle. Under some flight conditions, pressurized secondary injection may be required.

Another fluidic jet vectoring technique is Confined Jet Thrust Vector Control[7-9] (CJTVC). Similar to BLTVC, CJTVC uses an overexpanded nozzle, but the divergent portion of the CJTVC nozzle terminates in a constant area duct and then reconverges down stream to an orifice at the nozzle exit, thus creating a confined chamber that the overexpanded jet passes through before exiting. Small amounts of pressurized secondary air are injected into the confined chamber through ports on either side of the diverging portion of the nozzle. This causes the CJTVC jet to separate from that side of the nozzle similarly to the BLTVC. However, with the CJTVC, the separated jet follows the inside contour of the confined region of the system and so exits the orifice in a direction somewhat (dependent on the amount of separation) tangential to the interior contour at the orifice exit. While large vector angles were achieved with CJTVC, the vectoring could only be continuously varied over a fixed range. For a fixed amount of secondary injection air, there was a lower limit on the vectoring angle below which the vectoring jet was not stable. Additionally, unstable conditions and pressure fluctuations occurred in some cases where there was no secondary flow. These characteristics make the CJTVC scheme an unlikely candidate for aircraft applications.

Besides variable geometry and fluidic control, various other schemes for thrust vectoring have been explored. One notable study is that of Green and Glezer.[10] This study placed low power piezoelectric actuators at the exit of a rectangular nozzle. The actuators each vibrated a thin

sheet of steel at high frequencies. The tips of the steel sheets extended into the jet boundary where they excited the shear layer through their vibration. By actuating one side of the jet exit at a resonant frequency of 500 Hz, Green and Glezer showed that the jet could be vectored away from that side. This effect was achieved with little increase in cross-stream spreading. Further study is required to demonstrate the utility of this method for full scale thrust vectoring.

Still another method is the use of translating side walls of underexpanded nozzles as researched by Cornelius and Lucius.[11] This method employs a simple extension of a side wall on an underexpanded nozzle. Results indicated that a 20° vector angle in one direction was achievable for both 2-D and 3-D nozzle models. The study also indicated that such vectoring was possible with little loss in thrust efficiency. As with Green and Glezer's work, further study will be needed to show the applicability of the method to full scale.

Fluidic Counterflowing Nozzle

The fluidic nozzle concept employed in the present investigation is shown schematically in Fig. 1, which illustrates the side view of the short dimension of the jet. Collars are placed on either side of the primary flow nozzle (top and bottom in the figure) creating gaps between the exhausting jet and the collar surfaces which are curved away from the jet axis in the streamwise direction. To achieve upward thrust vectoring at an angle θ, as shown in Fig. 1, a secondary flow must be established in the upper shear layer of the jet. This is accomplished by activating a vacuum pump connected to the cavity between the primary nozzle and the upper collar. To assure stability it is important that this secondary *counterflowing* stream be applied to only one of the shear layers. Practically this is achieved by placing the collars between parallel side walls to minimize three-dimensional effects.

Anticipating the results to follow, it appears that the operation of the fluidic thrust vector nozzle shown in Fig. 1 depends on the shear layer entrainment characteristics of the two opposing shear layers which give rise to markedly different pressure distributions on the upper and lower collars during vectoring. This conjecture is based on studies[12-17] showing that the mixing and

entrainment characteristics of countercurrent mixing layers are fundamentally different than the more common coflowing arrangement. In particular, the turbulence levels measured in countercurrent mixing layers are significantly higher than those in coflowing layers providing a mechanism for the enhanced cross-stream momentum transport and pressure gradient. We will explore these connections in the sections to follow as the basic operation of the fluidic counterflowing nozzle is described.

Facilities

The experiments were conducted in the blow-down compressed air facility of the Fluid Mechanics Laboratory located at Florida State University. The facility is driven by a high-displacement reciprocating air compressor which is capable of supplying air at a maximum storage pressure of 160 bars (≈2300 psig). Owing to the significant tank pressure, the absolute humidity of the compressed air is extremely low, eliminating the necessity of drying the air prior to expansion in the supersonic nozzles. A series of large storage tanks provides a total capacity of 10 m^3 which is capable of driving the Mach 2 flow examined in this study continuously for up to 30 minutes. After leaving the storage tanks the air can be heated by passing through an array of resistive tank heaters having a maximum power output of 450 KW and capable of achieving stagnation temperatures T_0 up to 750 Kelvin. Operating the facility at elevated stagnation temperatures requires preheating the facility downstream of the tank heaters. This process bleeds the storage tanks by several hundred psi, but the overall run time is not significantly affected because the mass flow rate at Mach 2 is concomitantly reduced with increasing stagnation temperature. The stagnation pressure $P_0 = 7.928$ bar is held invariant to within 0.5% during each experiment using staged control values.

For the present study the blow-down facility was fitted with a rectangular nozzle having an exit aspect ratio of 4:1. The contour of the short dimension of the nozzle was generated by a method of characteristics for a design Mach number of two. The walls of the long dimension of the nozzle were parallel downstream of the throat and were blended to facilitate a transition from the

rectangular cross-section to the circular dimension of the connecting pipe upstream of the throat. The dimensions of the nozzle in the exit plane measured 13.0 mm by 52.0 mm and the throat area was 4.0 cm^2. During all experiments the stagnation to ambient pressure ratio across the nozzle was fixed as required for isentropically expanded flow at Mach 2. The jet was operated cold at a stagnation temperature of 300 K corresponding to an exit plane Reynolds number of 1.23×10^6 based on the short dimension of the jet. Hot supersonic flow was studied by elevating the stagnation temperature to 670 K, which produced a lower exit Reynolds number of 0.43×10^6.

The secondary flow stream illustrated in Fig. 1 was created by connecting a vacuum pump and manifold to a cavity which was carefully fitted to the upper shear layer of the jet. A similar arrangement was attached to the lower shear layer and isolated from the upper layer so that secondary flow could be applied independently on both sides of the jet. The regenerative vacuum pump was capable of developing 0.9 bar below atmospheric pressure (-13.4 psig) under no flow conditions. The mass flow rate of the secondary stream was obtained using a laminar flow meter located in the main supply line between the vacuum pump and collar. Internal dimensions of the collar arrangement are provided in Fig. 2. As outlined above the short dimension of the jet was H=13.0 mm and the width was W=52.0 mm. The height of the gap G measured in the jet exit plane between the nozzle lip and suction collar was varied in the present experiments between 3.5 mm and 9.5 mm, corresponding to $0.27 \leq G/H \leq 0.73$; the gap in the upper and lower collars were the same in all experiments. The contour of the collar shown in Fig. 2 is drawn to scale and was chosen through a preliminary study using a flexible collar arrangement. A more exhaustive parametric analysis which would be necessary to optimize the collar shape was considered to be beyond the scope of this investigation where the fundamentals of the fluidic thrust vector control were to be established. Fifteen pressure taps were positioned at equal intervals along the collar surface to capture the static pressure distributions; an additional tap was located in the jet exit plane and will be referenced at P_{exit}. Finally, side plates were fixed to the collar and extended downstream a distance L equal to 6.9 H. These plates were intended to minimize three-

dimensional affects and further isolate the action of the counterflow applied to only one of the jet shear layers during thrust vectoring.

Visualization of the jet was achieved by creating laser sheet images of the vectored plane along the jet axis using a pair of Spectra Physics frequency doubled Nd:YAG pulsed lasers. The lasers were fired simultaneously with a pulse energy of approximately 90 mJ each and a pulse width of 5 nsec. Fine condensation particles formed in the mixing region between the dry air of the cold jet and the moist ambient air were used for light scattering in a technique described by Clemens & Mungal[18], and captured on a Pentax 6x7 camera. Images of the entrained flow were also obtained to qualify the nature of the counterflowing stream along the upper shear layer of the jet. Here the laser sources were used to illuminate smoke which was introduced into the ambient gas surrounding the jet. To observe the smoke within the collars the laser sheet was passed through the lower collar surface which was manufactured from clear acrylic plastic. The side walls of the collar were also clear to capture the images on film. In the entrainment experiments the jet was heated sufficiently to eliminate light scattering from condensed water droplets but not enough to damage the clear acrylic collar and side walls.

Results and Discussion

We begin our discussion with a series of photographs taken in the vector plane of the jet showing the basic operation of the fluidic counterflowing nozzle. The images presented in Fig. 3 are 5 nsec exposures of the jet side view extending in the streamwise direction from approximately x/H of 7 to 23; the collar gap G was fixed at 5.0 mm. When the vacuum system connected to the upper collar is deactivated and air is allowed to entrain freely into both the upper and lower shear layers, the jet exhausts along its geometrical axis as shown in Fig. 3a. Under these conditions the collar arrangement operates analogously to a jet ejector configuration, albeit inefficiently due to the rapid divergence of the collar walls. Owing to fluid pumping in the secondary stream the exit plane static pressure, P_{exit}, registers a slightly negative value of -0.1 psig. The slight flapping motion of the jet seen if Fig. 3a is a consequence of weak pressure waves set up in the collar due to the

slightly underexpanded flow. (Recall that the stagnation pressure during the experiments is held fixed at a pressure ratio which assumes the jet is exhausting into atmospheric conditions for Mach 2 flow.)

When the vacuum system is activated creating counterflow in the collar, the jet can be vectored as shown by the photographs in Fig. 3b-d. The static exit pressures P_{exit} corresponding to the vector angles θ of 6°, 10°, and 16° varied between -0.9 psig, -2.2 psig, and -4.2 psig, respectively. We will demonstrate in the measurements to follow that the vector angle is a continuous function of P_{exit} and displays no hysteretic or bistable behavior. Furthermore, the mass flow rate of the secondary flow through the collar gap $\dot{m}_2$ is quite small and relatively insensitive to the vector angle itself. In the photographs of Figs. 3b-d the secondary mass flow rate is approximately 2% of the primary mass flow $\dot{m}_1$. Finally, the jet could be vectored toward either the upper or lower collar by activating the appropriate vacuum system. However, all the results presented below were made with the jet vectored up to reduce the possibility of damage to the lasers and optical components which were positioned below the jet.

To quantify the relationship between thrust vector angle and the secondary flow conditions the collar was instrumented with pressure taps as shown previously in Fig. 2. The collar pressures P_{collar}, obtained at T_o = 300 K for a gap of G=5.0 mm, are shown in Fig. 4. Each profile, referenced by P_{exit}, displays a relatively smooth static pressure distribution along the collar surface, with the exception of the data collected at station No. 8 where we believe a small leak may have developed resulting in the somewhat higher pressures measured there. The exit pressures were varied between -0.6 psig to -4.4 psig by throttling the main line between the vacuum pump and the collar.

The pressure distributions in Fig. 4 were integrated to obtain the resultant forces acting on the collar surface. These results, given in the table below, were used to estimate the thrust vector angle and thereby provide a comparison with the information obtained from the photographs. These calculations were made by balancing the vertical momentum and pressure forces acting on the collar and assuming the vectored jet momentum remains unchanged as it passes through the

control volume. Furthermore, estimates of the momentum of the secondary flow were made in the exit plane of the collar (i.e. at x=L) and were found to be insignificant compared to the primary jet momentum. At the maximum counterflow conditions of P_{exit} = -4.4 psig the momentum flux of the secondary stream was significantly less than 1% of the primary jet flow. Employing these assumptions the thrust vector angle of the jet was estimated using the expression $\theta = \sin^{-1}(F_y/\dot{M}_1)$, where F_y is the net vertical force acting on the collar and $\dot{M}_1$ is the momentum developed in the primary stream.

Integrated Pressure Data on Upper Collar

P_{exit} (psig)	F_x (Newtons)	F_y (Newtons)	θ, degrees
-0.6	5.2	22.0	3.3
-1.2	9.6	41.4	6.3
-2.2	13.1	61.2	9.3
-3.2	16.1	77.5	11.8
-4.4	19.3	96.5	14.8

Estimates of the thrust vector angle obtained by integrated collar pressure data were compared to the angles measured graphically from the photographs. These results are presented in Fig. 5 for the jet at T_0 = 300 K and a gap of 5.0 mm. Uncertainty estimates of the graphically determined angles were made by distributing sets of photographs at nominally identical conditions to four individuals and applying a t-test at a 90% confidence interval. The integrated collar data in Fig. 5 were obtained at P_{exit} values between -0.6 and -4.4 psig for both increasing and decreasing exit plane pressure. Studies of the directional sensitivity of the thrust vector angle to collar pressure were undertaken to determine whether hysteretic effects were associated with the fluidic nozzle operation. As the data suggest, we were not able to identify any directional dependence of the thrust vector performance under these operating conditions. This finding is quite encouraging given the history of fluidic elements to operate in a bistable manner. More will be said about this

feature of the operation when the basic operating mechanisms are discussed at the conclusion of the paper.

The performance curve in Fig. 5 indicates a unique and nearly linear relationship between vector angle and P_{exit} up to $\theta \approx 16°$. There are no indications from the present measurements that vector control beyond 16° should be problematic, the upper bound being determined entirely by the performance of our vacuum system. The agreement between the predictions of θ using collar pressure data and the photographs suggests that the assumptions employed in the momentum balance of the nozzle-collar system are reasonable. There will undoubtedly be losses associated with the non-ideal expansion caused by the cross-stream pressure gradient in the nozzle exit plane. These losses will lead to slight underpredictions of θ based on the integrated pressure data and may help explain similar underpredictions seen in the data of Fig. 5. Future work will incorporate a direct force balance to determine the nozzle performance and provide estimates of thrust efficiency.

Parametric effects

After establishing the basic operating characteristics of the fluidic counterflow nozzle, a preliminary parametric study was conducted to evaluate the sensitivity of thrust vectoring to simple alterations in collar geometry and the effect of increasing the jet stagnation temperature. We begin this section by addressing the issue of geometry and conclude with a summary of results taken in a supersonic hot jet.

The counterflow collars were designed to accommodate variations in gap width over a limited range of G between 3.5 mm and 9.5 mm. This was accomplished by translating the upper and lower collars in the vertical plane without variation in the collar contour itself. Care was taken during these experiments to position the collars symmetrically about the jet axis and to seal them to the side plates to eliminate leakage between the upper and lower jet shear layers.

Collar pressure profiles taken at P_{exit} = -3.4 psig for gap widths from 3.5 mm to 9.5 mm are presented in Fig. 6. Over a range of gap spacing between 5.0 and 9.5 mm the pressure profiles are relatively insensitive to the magnitude of G and fall on a smooth curve reminiscent of the trends

reported in Fig. 4. Estimates of the thrust vector angle for gaps between 5.0 and 9.5 mm using the momentum balance approach give $\theta = 13.2^{\circ} \pm 0.5^{\circ}$ (at 95% confidence). Collar pressure distributions obtained at other values of P_{exit} (not presented here) indicate that the fluidic nozzle performance is not significantly affected by gap spacing for all values of G tested between 5.0 and 9.5 mm. By contrast, the pressure profile at G=3.5 mm does not reach the relatively low vacuum pressures of the larger collar gaps for stations Nos. 2-10 and consequently results in a reduction in the thrust vector angle to 10.9°.

A closer examination of the nozzle operation at G=3.5 mm provides some insight into the anomalous behavior observed for small collar gaps. Pressure profiles measured at values of P_{exit} = -3.3, -4.6, and -6.0 psig are given in Fig. 7. The collar pressure rises monotonically at the lower levels of $-P_{exit}$ (3.3 and 4.6 psig) but the resultant force balance indicates that the thrust vector angle is consistently 15% lower than the value predicted by the performance curve of Fig. 5 obtained at the larger gap width of 5.0 mm. Flow visualization together with the collar pressure distributions were also used to verify the absence of hysteretic behavior for the 3.5 mm gap nozzle operated at $-P_{exit}$ less than 4.6 psig.

When the vacuum pressure in the nozzle exit plane is reduced slightly below -4.6 psig the jet becomes rather violent, displaying strong oscillations in thrust vector angle between approximately 13° and 23°. Eventually, when the pressure reaches -6.0 psig the jet stabilizes and is vectored at $\theta \approx 23^{\circ}$ generating a collar pressure distribution as indicated in Fig. 7. Under these conditions the collar pressure reaches a minimum value of -8.0 psig implying that the primary jet flow is attached to the collar in the neighborhood of station No. 6 and effectively acting as an ejector pump. It is likely that the counterflow mechanism is shut off under these extreme conditions returning the fluidic nozzle to an essentially bistable configuration. Additional work needs to be done here to document the details of the nozzle performance for small gap widths, in particular the hysteretic nature of the flow. At this stage of the research, however, we focused our attention on those conditions which appeared to be the most promising in achieving robust thrust vector control. The remainder of this report will be dedicated to those configurations.

A brief study was undertaken to assess the effectiveness of fluidic thrust vector control operated in a hot supersonic jet. These experiments were conducted by heating the primary jet to a stagnation temperature of 670 K and examining the vector response to variations in collar exit pressure P_{exit} while varying the gap spacing between 5.0 mm and 9.5 mm. At the elevated operating temperatures it was necessary to replace the clear acrylic side walls and lower collar with stainless steel components; the upper collar (including pressure tap arrangement) was unaffected by these changes.

Typical response curves of a hot supersonic jet to counterflow, compared to similar conditions in an unheated jet, are shown in Fig. 8 for a gap spacing of 5.0 mm. Pressure profiles taken at P_{exit} = -1.2 and -3.2 psig are in very close agreement over the forward third of the collar for hot and cold operating conditions. However, near station No. 5, the heated jet data depart from the cold profile leading to slightly lower sustainable vacuum pressures on the collar surface and consequently lower thrust vector angles. Estimated values of θ were 6.3° and 5.4° for cold and hot jet conditions, respectively, at P_{exit} = -1.2 psig. For operation at P_{exit} = -3.2 psig the respective cold and hot angles are 11.8° and 10.6°. The cause of the reduced performance in the hot jet is presently unclear but is probably related to the differences in the mixing layer dynamics of the two flows. The convective Mach number M_c of the cold and hot shear layer is 0.85 and 1.05, respectively. If we assume M_c is a relevant parameter in predicting at least the global features of the mixing layer within the collar, we can anticipate increased three-dimensional effects in the higher convective Mach number of the hot shear layer, which will affect the cross-stream pressure gradient near the collar. Detailed turbulence measurements of the velocity field within the collar must be obtained to resolve these and related issues.

Despite the differences in the shapes of the pressure profiles in Fig. 8 it is well to point out that the overall performance of the hot and cold jet are quite comparable as summarized in Fig. 9. Here we have collected all of the data obtained by integrating the collar pressure distributions and graphically using the flow visualizations. The open and closed symbols correspond to measurements made in cold and hot jets, respectively. We restricted the data in Fig. 9 to include

only collar gap conditions given by 5.0 mm $\leq G \leq$ 9.5 mm, where hysteretic effects were not observed. It is important to emphasize the relatively low scatter in the data indicating that the response of the fluidic nozzle is quite insensitive to changes in stagnation temperature and collar gap. We reiterate that the shape of the collar contour has not be systematically optimized, hence we expect that thrust vector performance can be improved.

The performance curve in Fig. 9 provides an effective summary of the operating characteristics of the fluidic thrust vector nozzle. The measurements indicate that thrust vector angles up to 20° can be expected over a range of operating conditions. The relationship examined between the jet exit pressure P_{exit} and thrust vector angle θ appears to capture the essential features of the nozzle operation. However, a more complete understanding of the mechanisms responsible for the thrust vector control is needed. In particular, we expect the unique characteristics of countercurrent mixing layers to play an important role in the jet dynamics in the collar region. In our earlier studies of countercurrent shear flows[12-14] we identified the velocity ratio U_2/U_1 as a critical parameter in determining the shear layer response to counterflow. Furthermore, we demonstrated that sufficient levels of counterflow give rise to shear layer self-excitation and concomitant increases in mixing and entrainment.

Here we provide a possible explanation of the basic operating principle of thrust vector control based on our understanding of countercurrent mixing layers. When the suction pump is activated on one side of the nozzle only, a reverse flowing stream can be established in the near field of the jet along one of the shear layers. When the velocity ratio of this counterflowing shear layer is increased above a threshold level, the mixing layer will become self-excited. We can expect that self-excitation will lead to the formation of well-defined two- and three-dimensional structures and elevated growth rates as observed in axisymmetric jets.[12-17] However, as these structures form in the upper shear layer of the rectangular jet, they will attempt to entrain mass, but this process will be inhibited by the presence of the collar in a manner analogous to the Coanda effect. Since a similar pumping mechanism is not active in the lower shear layer, the jet will be drawn off-axis resulting in jet vectoring.

Continuous control of the thrust vector angle can be attained in principle because the strength of the shear layer oscillations, and therefore entrainment rate, is a function of velocity ratio. However, one potential difficulty with the arrangement is the attachment of the primary jet to the collar leading to a bistable jet. In a bistable arrangement the thrust vector angle would be fixed, leading to a loss of control. Presumably the formation of a bistable jet can be prevented for the following reason. As the jet is drawn off axis and the cross-sectional area of the counte ng channel is reduced, there will be an increased pressure drop in the counterflowing stream. Consequently, the primary jet serves to choke the secondary stream reducing the counterflow and thus the effect of self-excitation. In this manner an equilibrium position will be achieved, where sufficient suction is present to excite the layer and cause jet vectoring, but not too large a vector angle such that the counterflow is cut off. A bistable configuration could only be maintained if sufficient vacuum pressure is present in the absence of counterflow to hold the jet against the collar.

We attempted to estimate the velocity ratio in the present experiments, but with some difficulty owing to the lack of quantitative information regarding details of the velocity field within the collar region. However, measurements of the mass flow ratio between the secondary and primary streams do provide some guidance. The data in Fig. 10 indicate that the mass flow ratio $\dot{m}_2/\dot{m}_1$ is relatively insensitive to P_{exit} and jet stagnation temperature, but does depend on the gap spacing G. The table below serves to summarize our results. We selected a set of operating conditions for hot and cold jets vectored at $\theta \approx 15^\circ$ (P_{exit}=-4.0 psig) using a representative geometry where G=5.0 mm.

Thrust Vector Performance
G = 5.0 mm
P_{exit} = -4.0 psig
$\theta = 15^{\circ}$

COLD JET (T_0=300 K)	HOT JET (T_0=670 K)
$\dot{m}_2/\dot{m}_1 = 0.02$	$\dot{m}_2/\dot{m}_1 = 0.02$
5 mm ≥ suction gap ≥ 1 mm	5 mm ≥ suction gap ≥ 1 mm
$0.09 \le U_2/U_1 \le 0.45$	$0.04 \le U_2/U_1 \le 0.21$
$0.0017 \le \dot{M}_2/\dot{M}_1 \le 0.0085$	$0.0008 \le \dot{M}_2/\dot{M}_1 \le 0.0042$

To compute the velocity ratio U_2/U_1 and momentum flux ratio $\dot{M}_2/\dot{M}_1$ using the measured mass flow rates, estimates must be made for the effective suction gap between the jet and collar wall through which the counterflowing fluid passes. We expected to gain some insight into this feature of the flow by introducing smoke into the ambient air surrounding the upper collar and thereby mark the entrainment of the secondary stream. The flow visualization in Fig. 11 indicates the nature of these studies for flow conditions at T_0= 400K, G = 5.0mm, and P_{exit} = -4.5 psig; the slightly elevated jet stagnation temperature was used to eliminate marking of fine condensation droplets in the shear layer present at lower temperatures. It can be observed that the smoke is readily drawn upstream into the collar, but also is carried downstream as it is entrained into the primary jet shear layer. This flow visualization technique was useful in verifying that ambient fluid was reaching the vacuum system, but was not particularly helpful in estimating the representative gap occupied by the secondary fluid, as the smoke is readily distributed across the entire mixing layer.

We chose instead to assume some reasonable values of the suction gap and compute the corresponding velocity and momentum ratios. For the conditions presented in the table above, the mass flow rate in the secondary stream was approximately 2% of the forward mass flow rate in both the hot and cold jets. Based on suction gaps between 1mm and 5mm the secondary velocity

and momentum flux were computed and included in the table. The calculations indicate that although the secondary velocity may be quite high if an extremely narrow gap existed between the vectored jet and the collar wall, the momentum flux of the secondary stream will be a small fraction of the forward jet momentum.

To summarize the findings of this initial study, we have shown that the thrust of supersonic hot and cold jets can be effectively vectored up to 16° by employing a fluidic counterflowing nozzle. The control is robust over a range of operating conditions and the thrust vector angle is approximately a linear function of the static pressure developed in the counterflowing stream. The principal advantage of the fluidic approach is the absence of moveable control surfaces, increasing the likelihood that the technology will move out of the laboratory. Future research must address a number of issues including: mult-axis thrust vector control; the forward flight effect; detailed measurements of the velocity field within the secondary stream; and dynamic testing to include time response issues. We believe the results of the present study demonstrate the utility of fluidic counterflow control and the value of continued research in this area.

Acknowledgments

The authors would like to express their thanks to the AFOSR for financial support of this research (contract F49620-92-J-0426) under the direction of Dr. James M. McMichael. We also appreciate the efforts of our students C.J. King, C. Ross, and M. Van der Veer.

References

[1] Doonan, J.G & Kuchar, A.P., "Scale model test results of a multi slotted 2-D/C-D ejector nozzle," AIAA Paper 92-3264, July 1992.

[2] Snow, B.H., "Thrust vectoring control concepts and issues," SAE Technical Paper Series, 901848, 1990.

[3] Capone, F.; Smereczniak, P.; Spetnagel, D. & Thayer, E., "Comparative investigation of multiplane thrust vectoring nozzles," AIAA Paper 92-3264, July 1992.

[4] Olsen, R.E., "Reattachment of a two-dimensional compressible jet to an adjacent plate," ASME Symposium on Fluid Jet Control Devices, 28 November 1962.

[5] Comparin, R.A.; et al., "On the limitations and special effects of in fluid jet amplifiers," ASME Symposium on Fluid Jet Control Devices, 28 November 1962.

[6] Warren, R.W., "Some parameters affecting the design of bistable fluid amplifiers," ASME Symposium on Fluid Jet Control Devices, 28 November 1962.

[7] Fitzgerald, R.E. & Kampe, R.F., "Boundary layer TVC for missile applications," AIAA Paper 83-1153, June 1983.

[8] Carrol, G.R. & Cox, H., "A missile flight control system using boundary layer thrust vector control," AIAA Paper 83-1149, June 1983.

[9] Porzio, A.J & Franke, M.E., "Experimental study of a confined jet thrust vector control nozzle," AIAA J. of Propulsion and Power, v. 5, no. 5, 1989, pp. 596-601.

[10] Green, S.M. & Glezer, A., "The manipulation of turbulent jets using surface-mounted actuators," AFOSR Grants 89-0465 & 92-J-0518, 1992.

[11] Cornelius, K.C. & Lucius, G.A., " Thrust vectoring control from underexpanded asymmetric nozzles," AIAA Paper 93-3261, July 1993.

[12] Strykowski, P.J. & Niccum, D.L., "The stability of countercurrent mixing layers in circular jets." *Journal of Fluid Mechanics,* Vol. 227, 1991, pp. 309-343.

[13] Strykowski, P.J. & Niccum, D.L., "The influence of velocity and density ratio on the dynamics of spatially developing mixing layers." *Physics of Fluids A,* Vol. 4, 1992, pp. 770-781.

[14] Strykowski, P.J. & Wilcoxon, R.K., "Mixing enhancement due to global oscillations in jets with annular counterflow."*AIAA Journal,* Vol. 31, No. 3, 1993, pp. 564-570.

[15] Strykowski, P.J. & Krothapalli, A., & Wishart, D., "The enhancement of mixing in high speed heated jets using a counterflowing nozzle." *AIAA Journal,* Vol. 31, No. 11, 1993, pp. 2033-2038.

[16] Strykowski, P.J. & Krothapalli, A., "The countercurrent mixing layer: strategies for shear layer control," AIAA 3rd Shear Flow Control Conference, paper AIAA-93-3260, Orlando, FL, 6-9 July, 1993.

[17] Krothapalli, A. & Strykowski, P.J., "Supersonic jet mixing: the role of streamwise vortices," Proceedings of Sixth ONR Propulsion Meeting, Boulder, CO, 31 Aug. - 2 Sept., 1993, pp. 159-164.

[18] Clemens, N.T. & Mungal, M.G., "A planar laser Mie scattering technique for visualizing supersonic mixing flows," *Exper. in Fluids*, Vol. 11, No. 2/3, 1991, pp. 175-185.

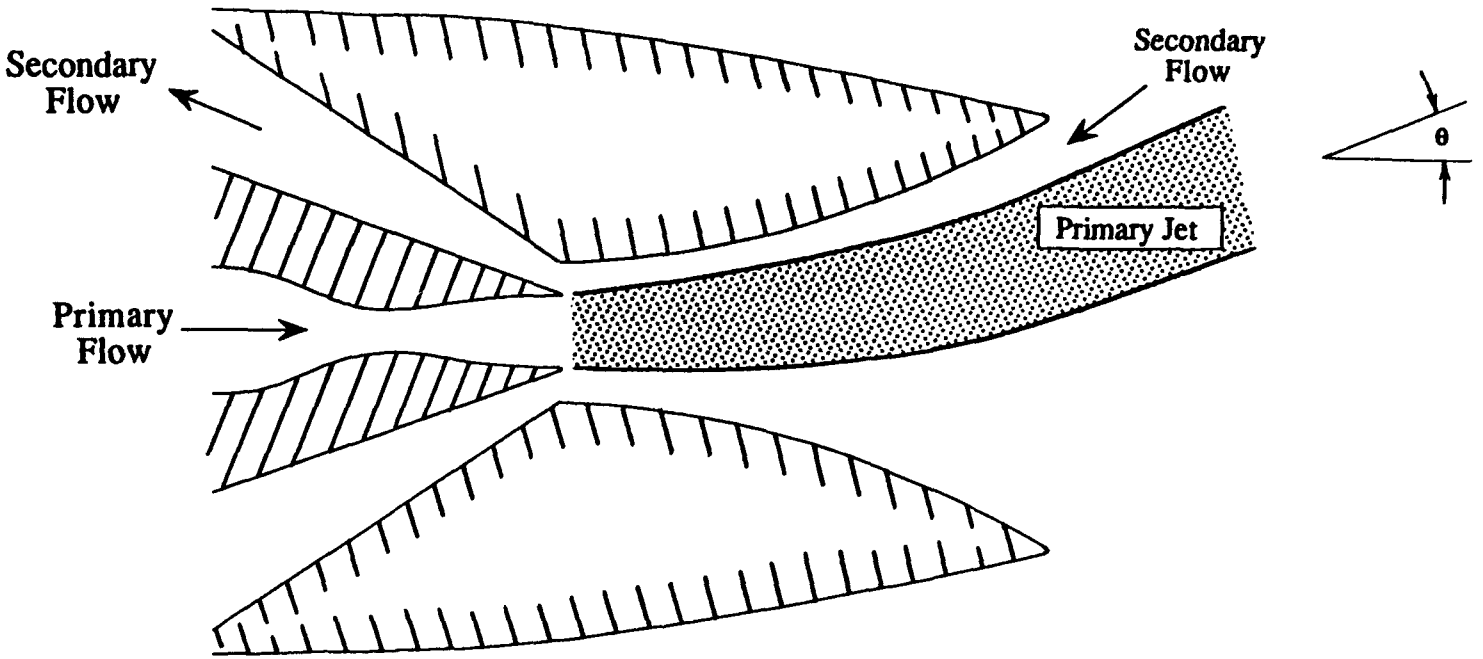

Figure 1: Schematic of fluidic thrust vector nozzle showing vectoring when counter-flow is activated in the upper shear layer of the jet.

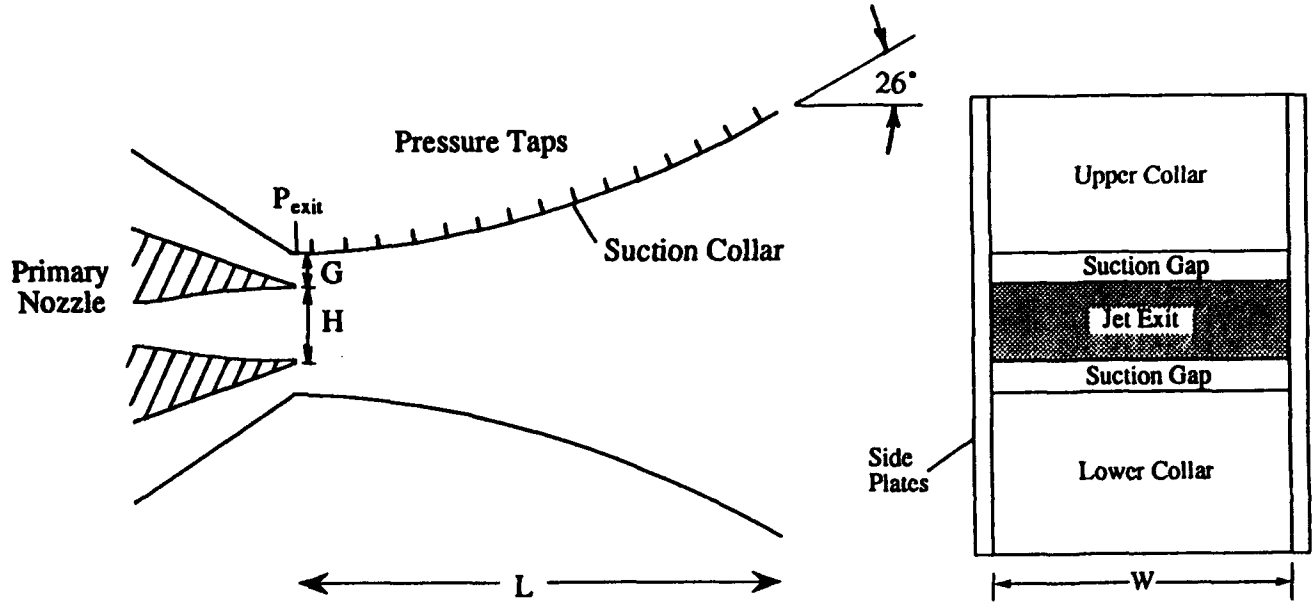

Figure 2: Scaled drawings of the internal dimensions of the side and end views of the nozzle-collar configuration.

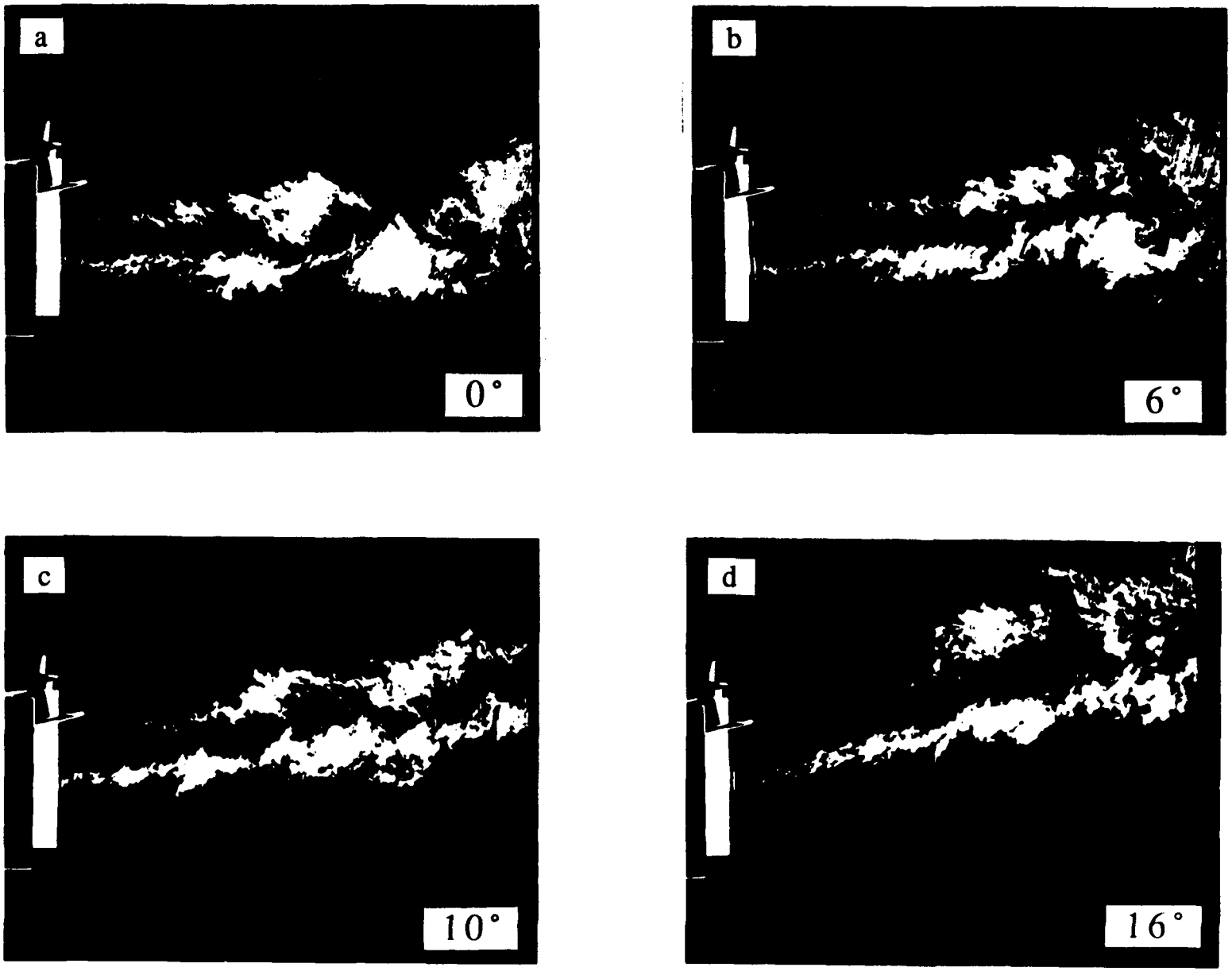

Figure 3: Condensation photographs of the side view of the jet showing thrust vectoring up to 16° using a collar gap of 5.0 mm.

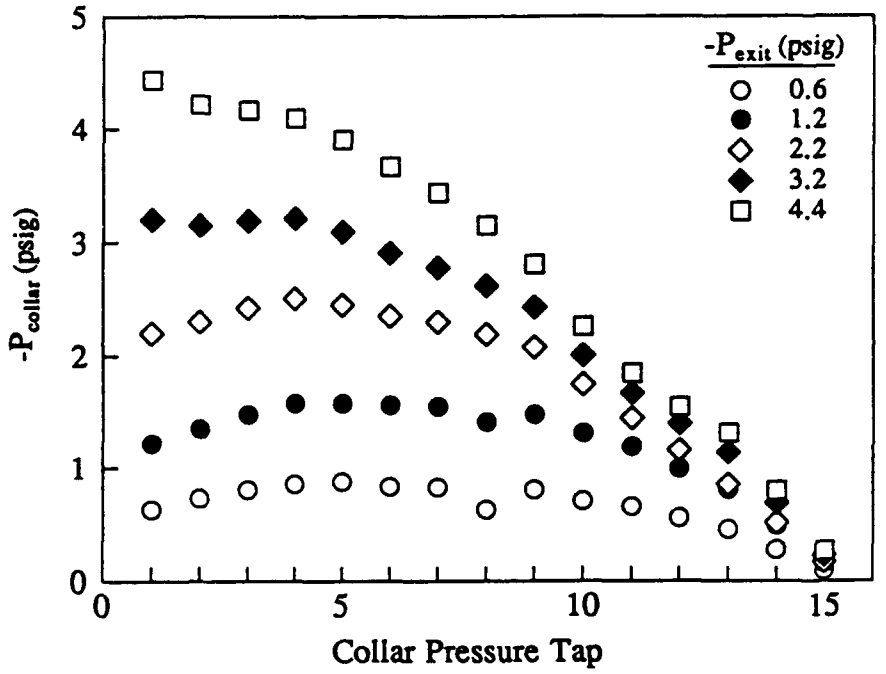

Figure 4: Collar static pressure profiles taken at T_o=300K for a gap of 5.0 mm.

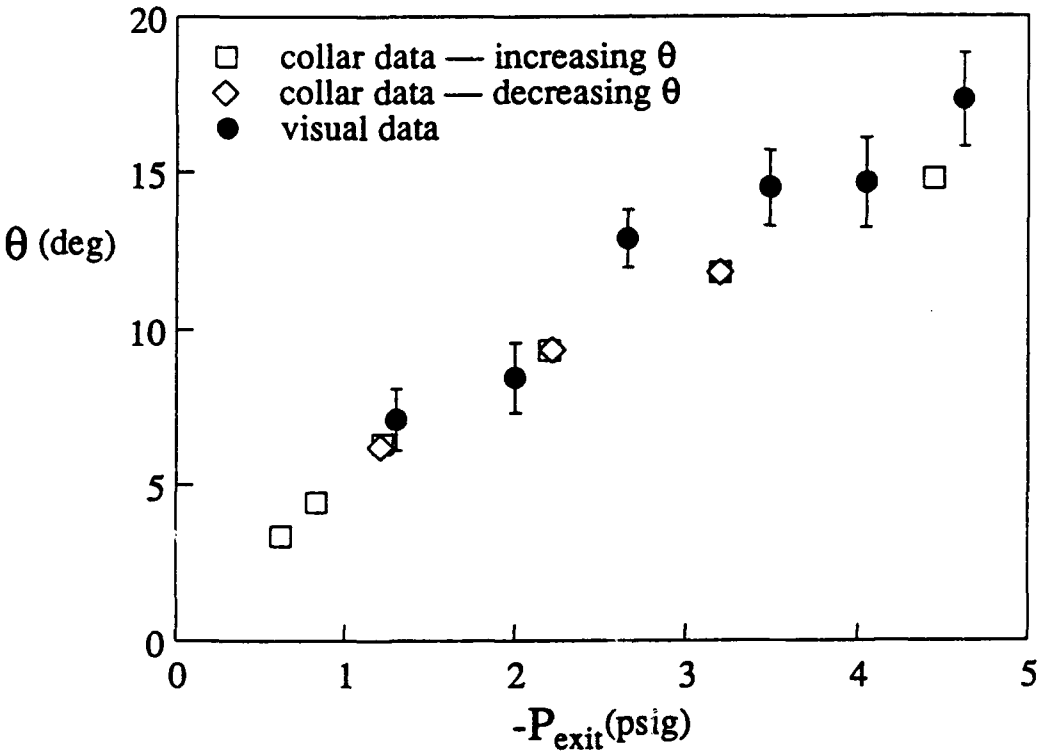

Figure 5: Thrust vector performance curve for T_o=300K and a gap of 5.0 mm.

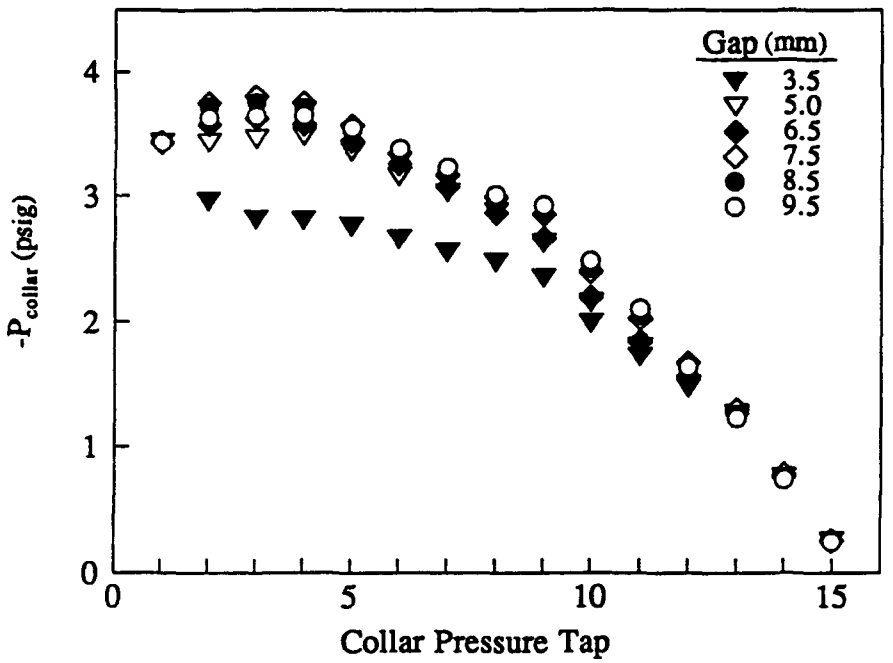

Figure 6: Collar static pressure profiles taken at T_o=300K and P_{exit}=-3.4 psig.

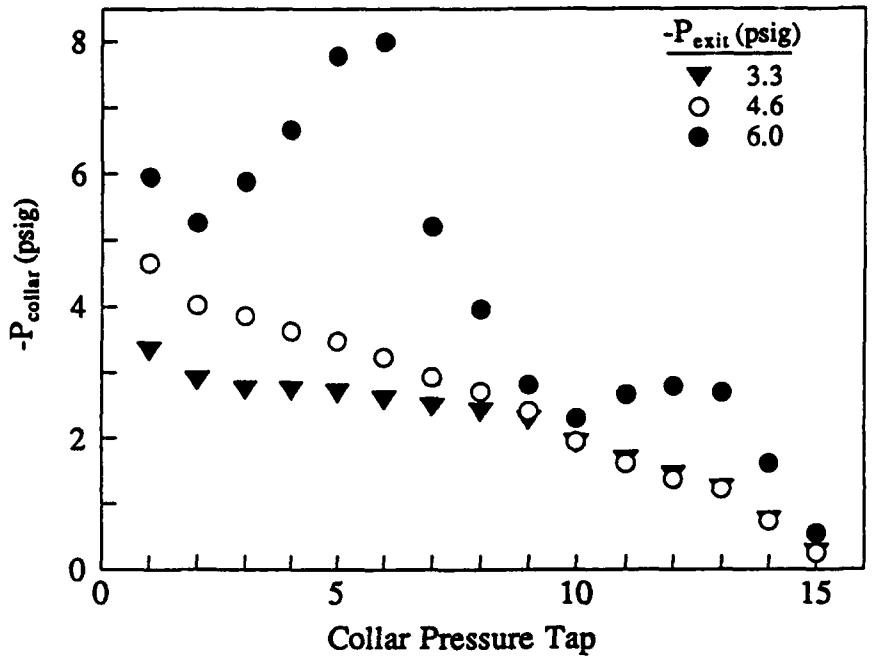

Figure 7: Collar static pressure profiles taken at T_o=300K for a gap of 3.5 mm.

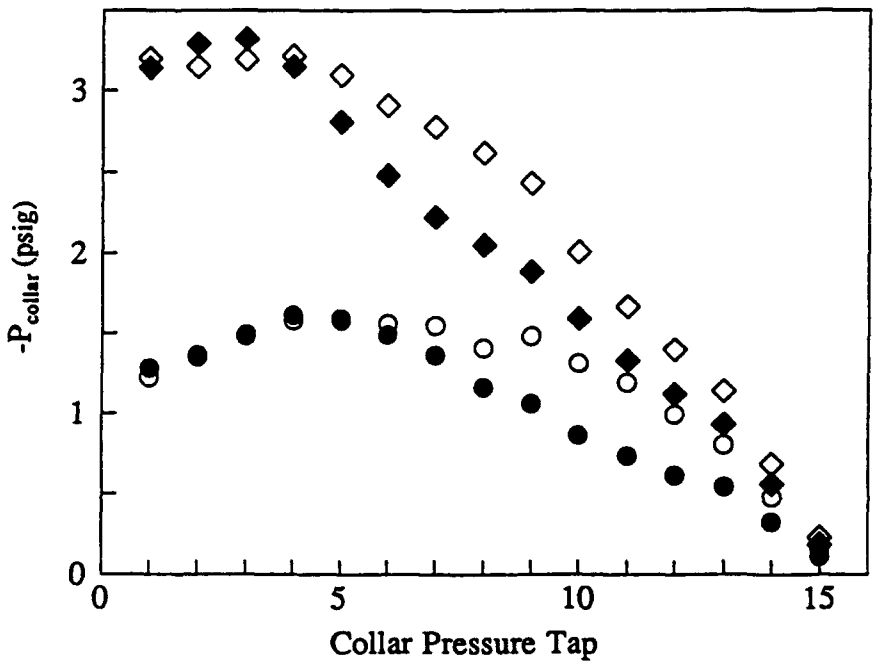

Figure 8: Collar static pressure profiles taken at P_{exit} = -1.2 and -3.2 psig for a collar gap of 5.0 mm. Open symbols indicate data collected at T_o=300K and solid symbols were taken at T_o=670K.

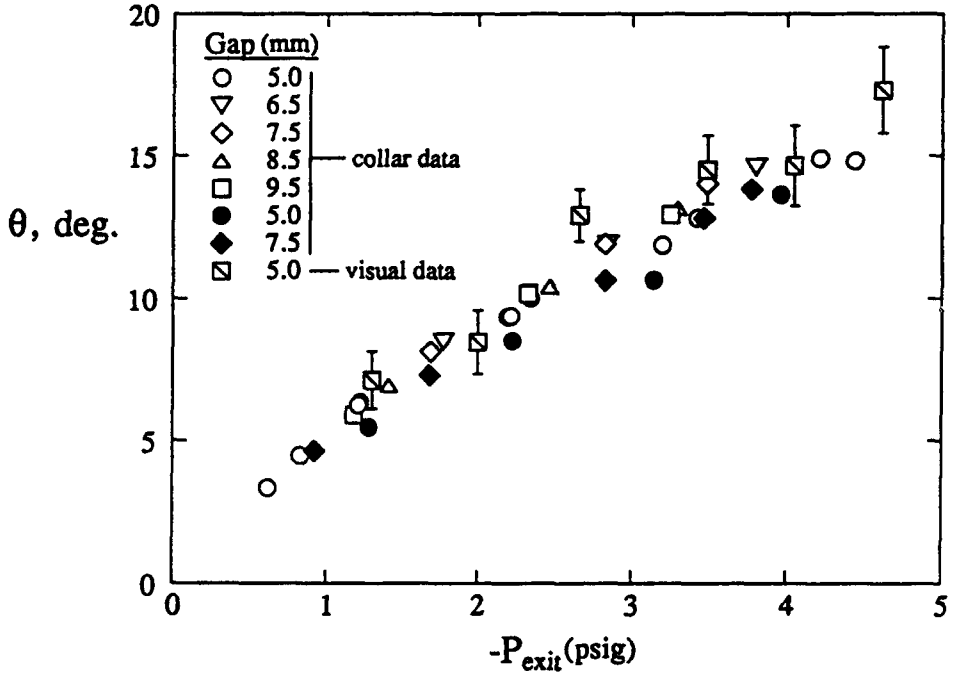

Figure 9: Thrust vector performance curve comparing nozzle operation for variable gap widths and jet stagnation temperatures.

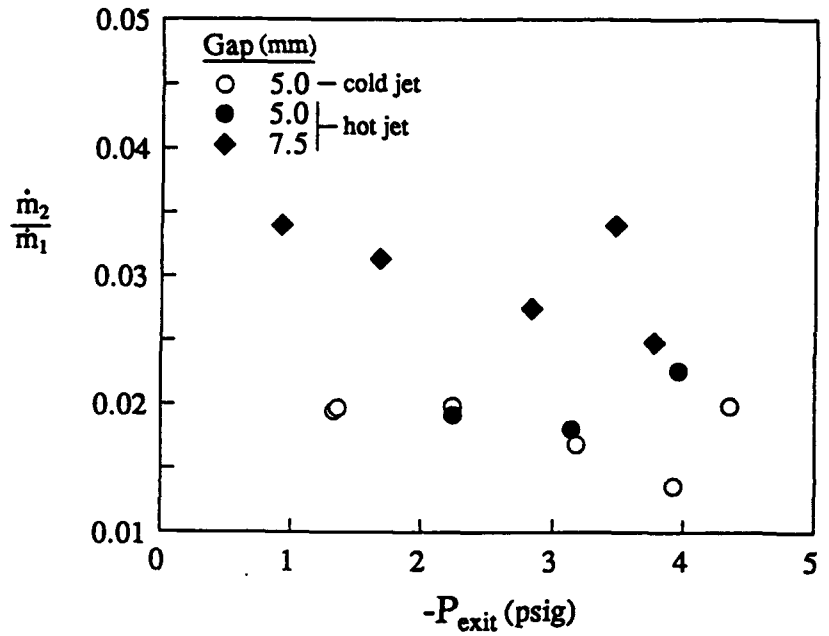

Figure 16: Dependence of mass flux ratio on collar gap and stagnation temperature.

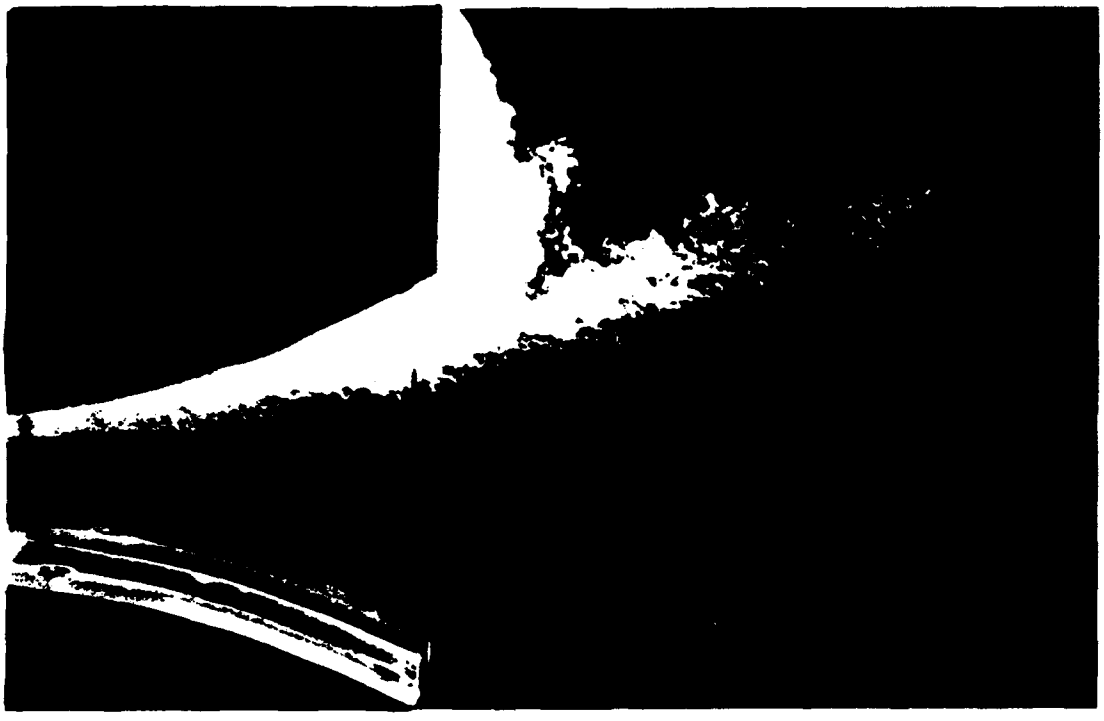

Figure 11: Flow visualization of the side view of the jet when smoke is entrained into the upper shear layer. The collar gap is 5.0 mm, P_{exit} = -4.5 psig, and T_o=400K.